Carbohydrate Polymers 90 (2012) 541–550

Contents lists available at SciVerse ScienceDirect

Carbohydrate Polymers

journal homepage: www.elsevier.com/locate/carbpol

Crystallization kinetics of poly(3-hydroxybutyrate-*co*-3-hydroxyvalerate)/cellulose nanowhiskers composites

Elena Ten[a], Long Jiang[b,*], Michael P. Wolcott[a,**]

[a] *Composite Materials and Engineering Center, Washington State University, Pullman, WA 99164-1806, United States*
[b] *Department of Mechanical Engineering, North Dakota State University, Fargo, ND 58102-6050, United States*

ARTICLE INFO

Article history:
Received 24 December 2011
Received in revised form 8 April 2012
Accepted 22 May 2012
Available online 30 May 2012

Keywords:
Crystallization
Nucleation
Nanocomposites
Cellulose nanowhiskers
Poly(3-hydroxybutyrate-*co*-3-hydroxyvalerate)

ABSTRACT

In this study, biodegradable poly(3-hydroxybutyrate-*co*-3-hydroxyvalerate) (PHBV) films with 1.2–4.6 wt% of cellulose nanowhiskers (CNWs) were manufactured by solution casting using *N*,*N*-dimethylformide (DMF) as the solvent. Crystallization behaviors of PHBV/CNW composites were studied under isothermal conditions using differential scanning calorimetry (DSC) and polarized optical microscopy (POM). The changes in PHBV crystalline structure were studied using wide angle X-ray diffraction (WAXD). Avrami analysis was performed to study the effects of CNW concentration and temperature on the crystallization rate and crystallinity of PHBV. POM study confirmed the results from the Avrami analysis. In particular, the results revealed the dual effects (i.e., nucleation and confinement) of CNWs on PHBV nucleation. Depending on the concentration of CNWs, the crystallization rate of PHBV could be either increased or decreased due to the combined effects. High crystallization temperatures increased the diffusion rate of PHBV chains and the growth rate of PHBV spherulites. However, the nucleation effect of CNWs decreased at high crystallization temperatures.

1. Introduction

Poly(3-hydroxybutyrate-*co*-3-hydroxyvalerate) (PHBV) is a semicrystalline copolymer naturally synthesized by bacteria. Due to its biodegradability and biocompatibility, PHBV has been studied extensively as a biodegradable plastic for many applications. However, wide-spread applications of PHBV are still hindered by several material drawbacks such as high material cost, poor thermal stability, brittleness and low crystallization rate. Numerous efforts have been made to overcome these drawbacks. Adding nucleating agents to PHBV is one route to increase crystallization rate of the polymer. Nucleating agents improve crystallization rates via heterogeneous nucleation by decreasing the surface free energy barrier. Various chemicals have been studied as potential PHBV nucleating agents, including boron nitride (BN) (Jiang, Huang, et al., 2008; Jiang, Morelius, Zhang, Wolcott, Holbery, 2008; Liu, Yang, Wang, Dong, & Liu, 2002; Qian, Zhu, Zhang, & Whitehouse, 2007; Weihua, Yong, & Yoshio, 2005; Withey & Hay, 1999), talc (Liu et al., 2002; Weihua et al., 2005), lanthanum oxide (La_2O_3) (Liu et al., 2002), terbium oxide (Tb_2O_3) (Liu et al., 2002), saccharin (El-Hadi, Schnabel, Straube, Muller, & Henning, 2002; Withey & Hay, 1999), phthalimide (Withey & Hay, 1999), thymine and melamine (Qian et al., 2007), α-cyclodextrin (He & Inoue, 2003), ammonium chloride (Figuly, 2004; Organ, Barham, & Webb, 1994), etc.

It was reported that one of the most effective nucleating agents for PHBV was boron nitride (Liu et al., 2002; Withey & Hay, 1999). It was able to reduce the degree of supercooling of a polymer and accelerate its crystallization. Jiang, Huang, et al. (2008) and Jiang, Morelius, et al. (2008) reported that the addition of 1 wt% of BN increased spherulite density and refined crystalline structure of PHBV8. The strength, elongation and impact toughness of the polymer increased after the addition of BN, while the modulus was slightly reduced.

The use of nanoparticles as nucleating agents is attractive because the particles can not only improve polymer crystallization but also increase mechanical and thermal properties of the composites. For example, inorganic nano-fillers such as multi-walled carbon nanotubes (Lai et al., 2004), silica (Ma et al., 2008; Xie, Kohls, Noda, Schaefer, & Akpalu, 2009), clay (Chen, Hao, Guo, Song, & Zhang, 2004; Ublekov, Baldian, & Nedkov, 2009), and layered double hydroxides (Dagnon, Chen, Innocentini-Mei, & D'Souza, 2009), have been shown to increase the crystallization rate of PHBV and the stiffness/thermal stability of the composites.

* Corresponding author. Tel.: +1 701 231 9512.
** Corresponding author. Tel.: +1 509 335 6392; fax: +1 509 335 5077.
E-mail addresses: long.jiang@ndsu.edu (L. Jiang), wolcott@wsu.edu (M.P. Wolcott).

0144-8617/$ – see front matter © 2012 Elsevier Ltd. All rights reserved.
http://dx.doi.org/10.1016/j.carbpol.2012.05.076

In particular, the effects of fumed silica and clay on the crystallization kinetics of PHBV were studied by Ma et al. (2008) and Chen et al. (2004), respectively. The results showed that the overall crystallization rate and crystallinity increased at low silica concentrations (≤2 wt%) and decreased at a high concentration (5 wt%). The authors suggested that when the content of silica was too high, it acted as large impurities and hindered crystallite growth. The crystallization process was controlled by the silica-promoted heterogeneous nucleation. Clay was found to show similar effects on PHBV crystallization.

Several studies on the production and properties of PHBV/cellulose nanowhiskers (CNWs) composites have been reported by our group (Jiang, Huang, et al., 2008; Jiang, Morelius, et al., 2008; Ten, Turtle, Bahr, Jiang, & Wolcott, 2010; Ten, Jiang, Bahr, Li, & Wolcott, 2012). CNWs are needle-like elementary crystals that occur naturally in cell walls of plants. It can be isolated using acid hydrolysis process (H_2SO_4 or HCl). We have shown that the CNWs in solution-cast PHBV/CNW composites increased the tensile strength, Young's modulus, and storage modulus of the composites. Tan δ peak was shifted to higher temperatures due to the PHBV–CNWs interactions at their interfaces. CNWs were also found to be an effective nucleating agent for PHBV. Siqueira et al. (2011) also demonstrated that CNWs drastically accelerated poly(ε-caprolactone) (PCL) crystallization. The lamellar growth computed from secondary nucleation theory decreased due to reduced mobility of the PCL chains.

Since CNWs play important roles in both crystallization and mechanical performance of PHBV, the objective of this research was to conduct an in-depth study on the influence of CNWs on the crystallization kinetics of PHBV. The effects of CNWs on the isothermal crystallization kinetics of PHBV were evaluated using Avrami analysis. PHBV spherulite growth rate and nucleation density were calculated based on POM observations.

2. Materials and methods

2.1. Materials

PHBV containing 12 mol% hydroxyvalerate (HV) was provided by Metabolix Inc. (Cambridge, MA). *N,N*-Dimethylformamide (DMF) was obtained from Acros Organics (Atlanta, GA). Microcrystalline cellulose (MCC) was supplied by Avicel (Type PH-102). Sulfuric acid (96 wt%) was purchased from J.T. Baker.

2.2. CNW preparation

MCC (1 g per 9.8 ml of acid) was mixed with 64 wt% sulfuric acid and the resultant suspension was stirred at 44 °C for 2 h. The suspension was diluted 10 times with deionized water and kept in a refrigerator to prevent further reaction. Sulfuric acid in the suspension was removed by repeated centrifuge (Sorvall, 5000 rpm for 5-min) until the supernatant was turbid. The supernatant (CNW suspension) was collected and dialyzed (Spectrum Laboratories Inc., molecular weight cutoff 12,000–14,000) against deionized water for 4–5 days to remove the remaining acid. When the suspension reached a constant pH value, it was removed from the dialysis tubes and neutralized with 1 wt% NaOH solution. The neutralized suspension was finally condensed at 80 °C using a Büchi Rotavapor (R-200) until the CNW concentration reached 2 wt%.

2.3. PHBV/CNW nanocomposites preparation

Various amount of condensed CNW suspension was added dropwise into 40 ml of DMF under continuous stirring. Water was evaporated from the mixture at 80 °C for an hour (DMF boiling temperature 153 °C) to obtain CNW/DMF suspension. 5 wt% of PHBV (based on the total weight of the CNW/DMF suspension) was added and the suspension was stirred at 80 °C until complete PHBV solution. The solution was sonicated for 5 min and then cast on a clean glass substrate. PHBV/CNW transparent films (thickness 15–30 μm) were obtained after overnight evaporation at 50 °C.

2.4. Characterization

2.4.1. Atomic force microscopy (AFM)

Morphology of cellulose nanowhiskers was investigated by an AFM. The tests were performed in tapping mode using a Veeco Multimode AFM equipped with a NanoScope IIIa controller (Digital Instruments Inc.). Prior to the tests, a drop of CNW suspension (in water) was deposited on freshly cleaved mica surfaces. The suspension was completely dried by evaporation at ambient temperature before being scanned by the AFM. The samples were scanned in air using Si tips (Digital Instruments Inc.) with a resonance frequency of ca. 330 kHz. The scan rate was 0.5 Hz.

2.4.2. Transmission electron microscopy (TEM)

The shape and size of CNWs were also studied by a TEM (JEOL 1200 EX) operating at 100 kV. Similar to the sample preparation method used for AFM, a drop of CNW water suspension was introduced on a formvar- and carbon-coated copper grid and the water was evaporated naturally. TEM images of CNWs were acquired without any sample staining.

To study the morphology of the PHBV/CNW composite films, small pieces of films were embedded in acrylic resin (London Resin Company Ltd.) and cured at elevated temperature overnight. Thin sections (50 nm thick) were cut from the resin with a glass knife using a Reichert-Jung ultramicrotome. The sections were placed on formvar coated copper grids and then stained with 2% uranyl acetate for 90 min.

2.4.3. X-ray diffraction (XRD)

Powder X-ray diffraction (XRD) was performed in reflection mode on a Phillips X'Pert diffractometer with an X'celerator detector using Ni-filtered Cu Kα radiation (λ = 1.5418 Å). The PHBV/CNW films were examined in the range of 2θ = 10–35° at 45 kV tension and 40 mA current at ambient temperature. XRD data was collected with a step size of 0.02° and count time of 50 s per point. A polycarbonate sample holder was used to avoid any peak overlap associated with the holder material.

2.4.4. Differential scanning calorimetry (DSC)

Isothermal crystallization of the neat PHBV and its nanocomposites was analyzed using a Mettler Toledo DSC 822e under N_2 flow (80 ml/min) with liquid nitrogen cooling. 5–10 mg samples were crimple-sealed in 40-μl aluminum crucibles and heated from room temperature to 200 °C at 10 °C/min. The temperature was maintained for 2 min to remove any prior thermal history. The samples were subsequently cooled rapidly at 100 °C/min to predetermined crystallization temperatures (T_c = 50, 60 and 70 °C) and then kept isothermal for 15 min. Heat flow was measured during the isothermal crystallization. Three replicates were performed for each formulation.

2.4.5. Polarized optical microscopy (POM)

Isothermal crystallization behavior of the samples was studied by an Olympus BX51 POM equipped with a Linkam hot stage (THMS600/HFS91). Sample films were sandwiched between two glass slides and heated up to 220 °C. The films were equilibrated for 10-min to eliminate any residual PHBV crystallization seeds

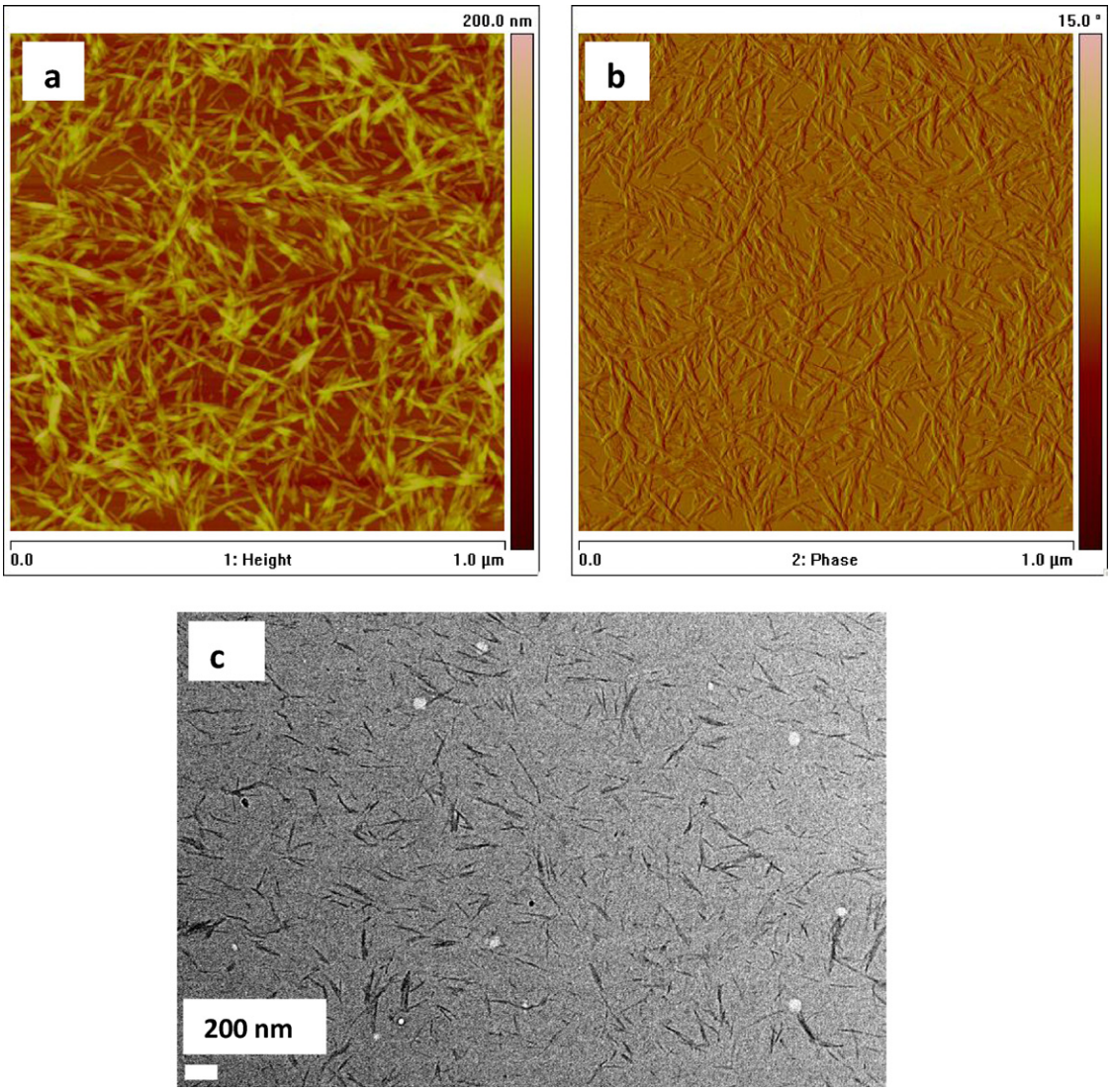

Fig. 1. Morphology of CNWs. (a) AFM topography; (b) AFM phase image; (c) TEM micrograph.

and then quenched in liquid nitrogen to obtain complete amorphous samples. The amorphous films were studied for PHBV nucleation and spherulite growth at 50, 60 and 70 °C using the POM. Sequential images of PHBV spherulites were taken by an attached digital camera every 3 s. Spherulite radii R were measured using SPOT Advanced software (Diagnostic Instruments Inc.).

3. Results and discussion

3.1. Morphology of CNWs and PHBV/CNWs composites

The shape and size of CNWs were shown in AFM and TEM micrographs (Fig. 1). The aspect ratio of the nanowhiskers was determined based on the measurements of 300 individual whiskers from the TEM micrographs using ImageJ software (National Institute of Health). The average aspect ratio was found to be 18 ± 7.5 (Ten et al., 2012).

Fig. 2 shows TEM images of PHBV/CNW composites comprising different concentrations of CNWs. It can be seen that CNWs were dispersed evenly in the PHBV matrix at 2.3 wt% concentration (Fig. 2a). CNW agglomeration occurred and intensified with increasing CNW concentration (Fig. 2b and c).

3.2. XRD analysis of PHBV/CNW composites

X-ray diffraction 1D patterns of the neat PHBV and PHBV/CNW composite films are shown in Fig. 3. The very similar structures of PHB and PHV homopolymers result in PHBV exhibiting isodimorphism (Kamiya, Sakurai, Inoue, Chujo, & Doi, 1991). PHBV copolymers with less than 40 mol% HV units crystallize within the PHB crystalline lattice (Chan, Kummerlöwe, & Kammer, 2004) and display the same diffractograms as the PHB homopolymer (Bloembergen, Holden, Hamer, Bluhm, & Marchessault, 1986; Owen, Heinzel, Škrbić, & Divjakovic, 1992). The PHBV used in this research had 12 wt% HV content and therefore had the same orthorhombic crystal structure as PHB (Miao, Qiu, Yang, & Ikehara, 2008). Typical diffraction peaks at ca. 13.4° and 16.0° are attributed to (0 2 0) and (1 1 0) crystal planes, respectively (Miao, Qiu, Yang, & Ikehara, 2008). It can be seen from Fig. 3 that (0 2 0) peak become sharper and more intense with CNWs content, suggesting that nanowhiskers increased the ordering level of PHBV molecular chains. The increases in (0 2 0) peak intensity also suggested that nanowhiskers increased PHBV crystallinity.

The interplanar distance d of a crystal structure is determined by Bragg's law:

$$n\lambda = 2d \sin\theta, \quad (1)$$

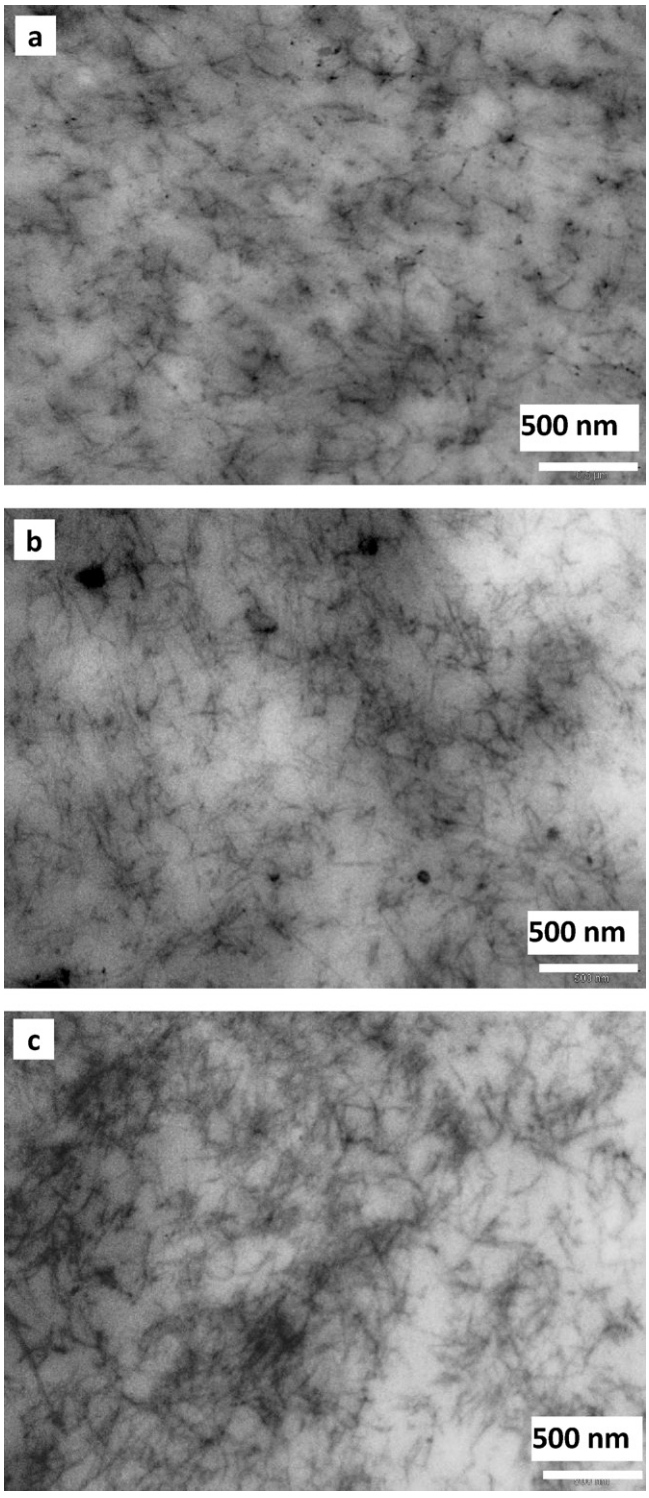

Fig. 2. TEM images of PHBV/CNW composites comprising 2.3% (a), 3.3% (b), and 4.6% (c) of CNWs.

where n is the reflection number (integer), θ is the angle of the diffracted beam and λ is the wavelength. The interplanar distance is a function of Miller indexes ($h\,k\,l$) and the lattice parameters (a, b, c). The relationship between d and the lattice parameters is given by:

$$d = \frac{1}{\sqrt{(h^2/a^2 + k^2/b^2 + l^2/c^2)}}, \quad (2)$$

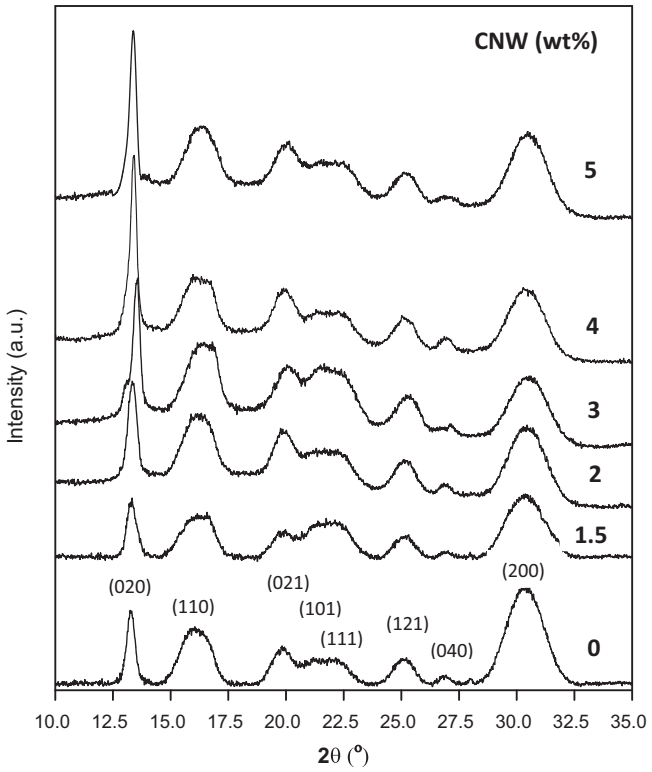

Fig. 3. X-ray diffraction pattern of neat PHBV and randomly oriented PHBV/CNW composites.

The crystalline lattice parameters of neat PHBV were calculated from the (0 2 0), (1 1 0) and (0 2 1) diffraction peaks corresponding to 13.4° (d = 6.6 Å); 16.8° (d = 5.3 Å) and 20° (d = 4.4 Å), respectively. The parameters a = 5.748 Å, b = 13.20 Å, and c = 5.904 Å were in good agreement with the results reported previously for PHBV12 (Hirota, Yoshie, Ishii, Kasuya, & Inoue, 2005).

Fig. 3 also shows that no additional PHBV diffraction peaks occurred after the addition of CNWs, indicating that the nanowhiskers did not cause new crystalline symmetries of PHBV. CNWs, on the other hand, were reported to show three diffraction peaks at ca. 14.5°, 16.4° and 22.5°, representing (1 $\bar{1}$ 1), (1 1 0) and (2 0 0) planes, respectively (Martínez-Sanz, Olsson, Lopez-Rubio, & Lagaron, 2011; Sugiyama, Vuong, & Chanzy, 1991; Tokoh, Takabe, Fujita, & Saiki, 1998). The strongest peak, characteristic of cellulose I, is located at 22.5° and can be recognized even at low CNW concentrations (Fig. 4). Furthermore, it can be seen from Fig. 4 that the positions of the (1 0 1) and (1 1 1) diffractions of PHBV (21.5° and 22.3°, respectively) shift to higher angles after the addition of CNWs, an indication of PHBV crystalline structure change induced by the nanowhiskers. These changes occurred because the PHBV formed defective crystals in the presence of CNWs. These CNWs hindered chain diffusion and folding during PHBV spherulitic growth.

Crystal dimension D_{hkl} in the direction perpendicular to the diffracting planes can be determined using Scherrer's equation (Klug & Alexander, 1954):

$$D_{hkl} = \frac{0.9\lambda}{\beta_{1/2}\cos\theta}, \quad (3)$$

where θ is the diffraction angle, λ is the wavelength and $\beta_{1/2}$ is the peak width of half intensity (in radians) prior to smoothing. D_{hkl} was calculated using the diffraction peak at ca. 30.5°, i.e., the (2 0 0) plane of PHBV. The results (Table 1) show that the apparent crystal size D_{hkl} was smaller in the composites than in the pure

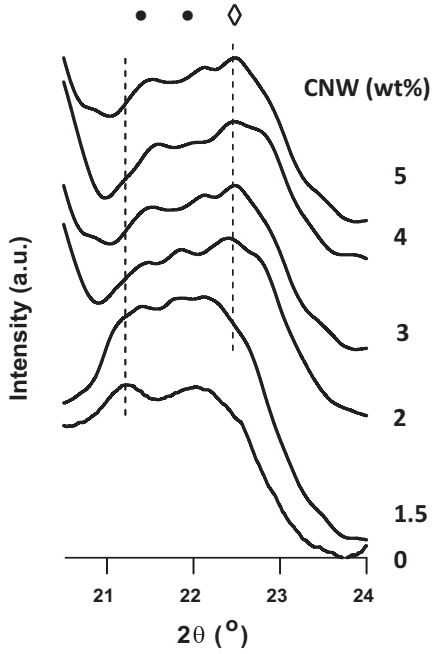

Fig. 4. X-ray diffraction patterns of PHBV and PHBV/CNW composites over $2\theta = 20.5–24^{\circ}$. ● Indicates (1 0 1) and (1 1 1) PHBV crystal planes and ◊ – (2 0 0) CNW crystal plane. Data were smoothed over 25 adjacent points.

PHBV, implying that CNWs hindered the diffusion and folding of PHBV chains due to the confinement effects of the nanowhiskers (Zhang, Yu, Zhou, Chen, & Hu, 2010; Zhou, Chu, Wu, & Wu, 2011). Moreover, PHBV/1.5CNW and PHBV/2CNW showed the smallest D_{hkl}, indicating the strongest confinement effects in these two composites. This was because CNWs were homogeneously dispersed in PHBV (meaning large interfacial areas between CNWs and PHBV) at low concentrations as revealed by TEM observations (Fig. 2) and mechanical properties assessments (Ten et al., 2010). The refined crystal structures could contribute to improved mechanical properties of the composites.

3.3. Isothermal crystallization kinetics of neat PHBV and PHBV/CNW composites

The crystallization kinetics combining nucleation and growth effect can be analyzed using the Avrami equation (Avrami, 1939):

$$1 - X_t = \exp(-kt^n), \tag{4}$$

or

$$\log[-\ln(1 - X_t)] = n\log(t) + \log(k), \tag{5}$$

where X_t is the relative degree of crystallinity at time t, n – Avrami exponent which depends on nucleation and growth mechanisms, k – overall crystallization rate constant. Nucleation rate and spherulite linear growth rate are assumed to be constant in the equation (Lorenzo, Arnal, Albuerne, & Muller, 2007). Nucleation and spherulite growth are separate phenomena, but they are both influenced by the same processing parameters such as temperature. Avrami exponent n is determined as the dimensionality of the growing crystals.

X_t is given as:

$$X_t = \frac{\int_0^t (dH/dt)dt}{\int_0^\infty (dH/dt)dt}, \tag{6}$$

The numerator is the heat flow after time t and the denominator is the total heat flow during crystallization. Induction time ($t = 0$) was determined by a flat baseline after the initial spike on a DSC curve (Lorenzo et al., 2007).

Fig. 5 shows X_t as a function of the crystallization time t at different crystallization temperatures. DSC measurements at 30, 40, and 80 °C did not show any crystallization peak within the measurement periods and therefore their curves are not shown in the figure. This is most likely because these three temperatures are out of the cold crystallization range of PHBV. It can be seen from Fig. 5 that CNW content had different effects on PHBV crystallization at different temperatures. For instance, at 50 °C, the sigmoidal isotherms were shifted to the left after the addition of different concentrations of CNWs, indicating faster crystallization process (Fig. 5a). In particular, PHBV/2.3% CNW composite crystallized 7 times faster compared to the neat PHBV (crystallization time decreased from 12 min to 1.7 min). At $T_c = 60$ °C PHBV/CNW composites (at all CNW concentrations) still crystallized faster than unfilled polymer, but their rate difference was much smaller compared to $T_c = 50$ °C (Fig. 5b). At $T_c = 70$ °C, the composites containing 2.3 and 3.3% CNWs crystallized slower than did the neat PHBV. On the contrary, the composites containing 1.2 and 4.6 wt% CNWs still crystallized faster than did the neat polymer. It is unclear why the crystallization rate was reduced when 2.3 and 3.3% CNWs were added. Neat PHBV had a cold crystallization temperature (T_{cc}) of 55 °C (Ten et al., 2010, 2012). The crystallization rate of PHBV diminished at temperatures lower or higher than this temperature. Lower-than-T_{cc} temperature makes chain diffusion and folding difficult and higher-than-T_{cc} temperature reduces polymer nucleation (discussed further in Section 3.4). CNWs increase overall crystallization rate of PHBV by acting as a nucleation agent to increase polymer nucleation rate (Ten et al., 2010, 2012). Therefore at the temperatures higher than T_{cc} (e.g. 60 and 70 °C in this study), the nucleation effect of CNWs was reduced and the overall crystallization rate at these two temperatures was less affected by CNWs than at 50 °C.

The overall crystallization rate can be calculated using the following equation:

$$G = \frac{1}{t_{0.5}}, \tag{7}$$

where the half time crystallization $t_{0.5}$ is the time when X_t reaches 50%. It can be directly determined from X_t data (Fig. 5) or be calculated using this equation:

$$t_{0.5} = \left(\frac{\ln 2}{k}\right)^{1/n} \tag{8}$$

where k and n are obtained from the Avrami equation. Fig. 6 shows the variation of G as a function of CNW concentration at different temperatures. The largest variation of G was demonstrated at 50 °C due to the temperature influence on the nucleation effect of CNWs. Although the three curves in Fig. 6 differ from each other markedly, they share a common trend, i.e., G increased with increasing CNW content at low CNW concentrations, decreased at medium concentrations and eventually started to increase again at high concentrations. CNWs provided heterogeneous nucleation sites for PHBV crystallization and therefore increased its overall

Table 1
Apparent crystal size (D_{hkl}) of PHBV and PHBV/CNW composites.

CNW (wt%)	D_{hkl} (nm)
0	32.1
1.5	12.85
2	12.86
3	16.1
4	18.4
5	16.1

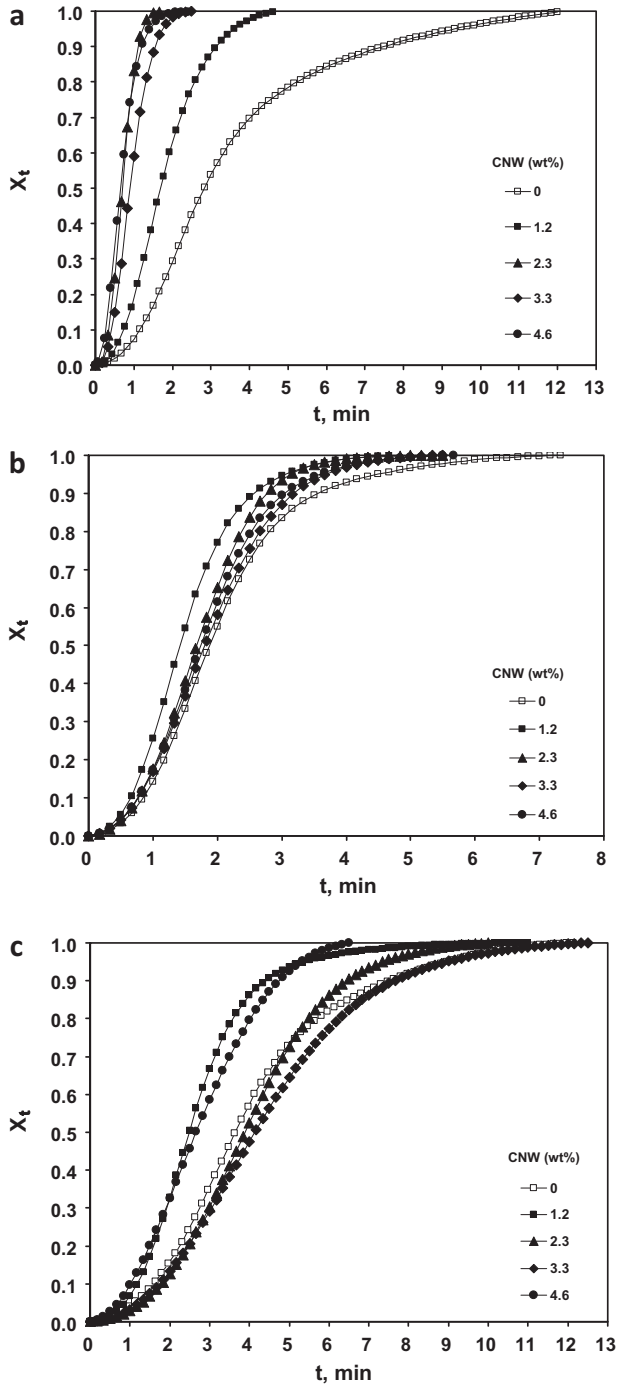

Fig. 5. Relative crystallinity X_t versus isothermal crystallization time of PHBV and PHBV/CNW composites at crystallization temperatures: (a) 50 °C; (b) 60 °C; (c) 70 °C.

crystallization rate at low CNW concentrations. On the other hand, CNWs can restrict PHBV chain mobility through their interfacial interactions with the polymer. This confinement effect has been demonstrated by low frequency solid-like behavior in rheological tests, broadened relaxation peaks and increased moduli at high temperatures in DMA tests (Ten et al., 2012). The confinement can hinder the diffusion of polymer chains into crystalline lattice; hence decelerate the growth of PHBV spherulites. In the medium CNW range, this confinement effect could overweigh the nucleation effect of CNWs and therefore decreased the overall crystallization rate (Li, Li, Ni, Rong, & Hsiao, 2007). CNW agglomeration started to occur when its concentration exceeded an optimum homogeneous

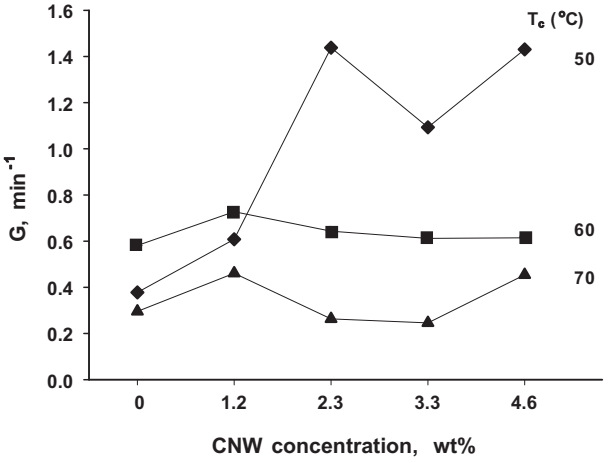

Fig. 6. Overall crystallization rate G of PHBV and PHBV/CNW composites at different crystallization temperatures.

CNW dispersion state, which was estimated to be at CNW ~2.3% from one of our previous studies (Ten et al., 2012). This agglomeration can also be noticed from the TEM micrographs shown in Fig. 2. The agglomeration reduced the confinement effect of CNWs and allowed PHBV spherulites to grow faster and bigger. Therefore, G tended to increase again at high CNW concentrations. The nucleation and confinement effects of CNW concentration on PHBV crystallization was also confirmed by POM micrographs discussed later.

High crystallization rate does not necessarily mean high degree of crystallinity. The absolute degree of crystallinity of PHBV/CNWs samples can be derived from the overall heat flow of the complete crystallization process:

$$X_c = \frac{\Delta H_c}{(1-\varphi)\Delta H_m}, \quad (9)$$

where ΔH_m is heat of fusion of the PHBV with 100% crystallinity (146 J/g) (Barham, Keller, Otun, & Holmes, 1984), φ – CNW mass fraction in PHBV/CNW composites, ΔH_c – heat of fusion of the sample. Fig. 7 displays the dependence of X_c on CNW concentration for the neat PHBV and PHBV/CNW composites at different crystallization temperatures. Overall, the crystallinity increases with increasing crystallization temperature, which is opposite to the trend of the crystallization rate shown in Fig. 6. The high crystallization rate at 50 °C was the result of the strong nucleation effect of CNWs at this temperature. However, the temperature is not ideal for spherulitic growth. The spherulites produced at this low

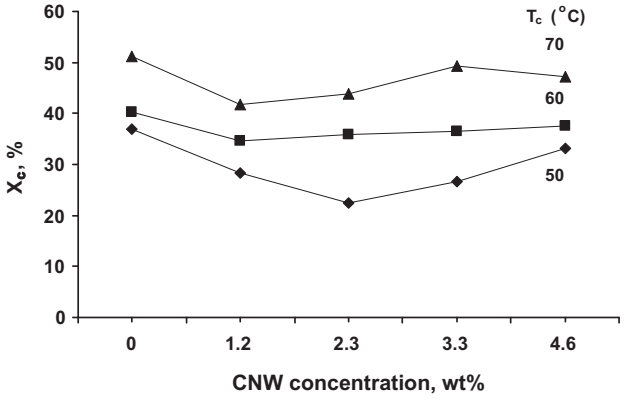

Fig. 7. The absolute degree of crystallinity X_c of PHBV and PHBV/CNW composites at different crystallization temperatures.

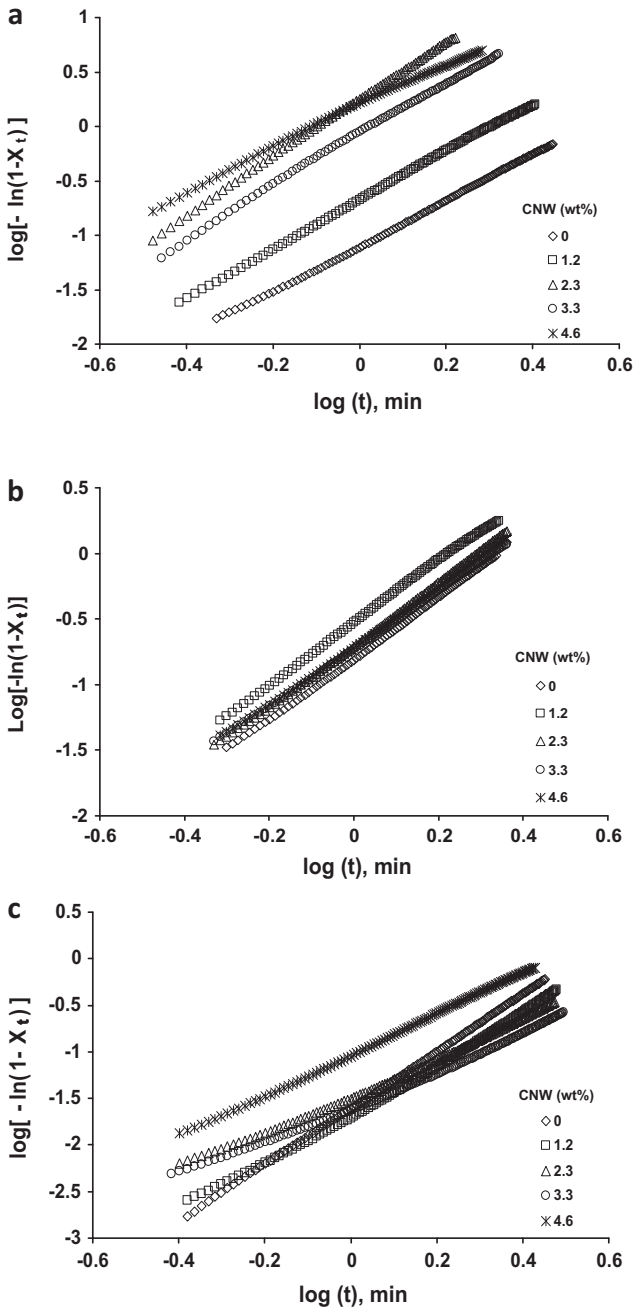

Fig. 8. Avrami plots of PHBV and PHBV/CNW composites crystallized at 50 °C (a), 60 °C (b), and 70 °C (c).

temperature could be defect-ridden with low laminar thickness due to slow PHBV chain diffusion. This type of spherulites exhibited low heat of fusion, hence the samples showed low X_c. On the contrary, although higher temperatures (i.e., 60 and 70 °C) resulted in decreased CNW nucleation effect and lower crystallization rate, large spherulites with more perfect structures could be obtained (within a longer period of time compared to T_c at 50 °C) due to higher level of chain mobility. These spherulites had high heat of fusion and therefore resulted in samples with high X_c.

Avrami plots for the PHBV/CNWs samples at different crystallization temperatures are shown in Fig. 8. Avrami exponent n and overall crystallization rate constant k can be deduced from the slope and the intercept of the lines, respectively. The obtained values are listed in Table 2. Avrami exponent n varied from 2.24 to 2.89 depending upon CNW concentration and crystallization

Table 2
Kinetic parameters for isothermal crystallization of PHBV and PHBV/CNW composites crystalized at 50, 60, and 70 °C.

Temperature (°C)	CNW (wt%)	n	$k \times 10^2$ (min^{-n})	$t_{0.5}$ (min)	X_c (%)
50	0	2.24 ± 0.1	7.84	2.64	37
	1.2	2.40 ± 0.1	21.01	1.64	28
	2.3	2.59 ± 0.09	177.58	0.69	23
	3.3	2.42 ± 0.01	85.96	0.91	27
	4.6	2.29 ± 0.05	157.40	0.69	33
60	0	2.74 ± 0.04	15.68	1.72	40
	1.2	2.67 ± 0.07	29.66	1.37	35
	2.3	2.85 ± 0.13	24.14	1.55	34
	3.3	2.67 ± 0.18	18.68	1.63	36
	4.6	2.62 ± 0.06	19.38	1.62	38
70	0	2.73 ± 0.46	2.49	3.38	51
	1.2	2.62 ± 0.13	9.11	2.17	42
	2.3	2.89 ± 0.05	1.46	3.8	44
	3.3	2.50 ± 0.14	2.08	4.07	49
	4.6	2.42 ± 0.15	10.25	2.2	47

temperature (Table 2). For predetermined (i.e., nucleation agent added) three-dimensional crystallization a theoretical value of 3 should be obtained for n. The lower-than-3 n values in the table could be due to mixed sporadic and predetermined crystallization and/or mixed 3D and 2D crystallization (because the samples were confined between two glass slides). Moreover, the changes in Avrami exponent after the addition of nanowhiskers indicate that the presence of CNW modified the growth pattern of PHBV crystals. The nucleation effect of CNWs, their confinement on PHBV crystal growth, and the impingement effect between densely packed crystals after the addition of CNWs; all these factors likely influenced the final value for n. The influence of these factors on n could have resulted through a modification in the crystallization type (sporadic/predetermined/mixed) and crystal growth dimensions during PHBV crystallization.

The crystallization rate parameter k increased with decreasing crystallization temperature for all formulations studied (Table 2). This trend is in agreement with the overall crystallization trend shown in Fig. 6. At the same crystallization temperature, k followed the same trend of the overall crystallization rate G, exhibiting an increase–decrease–increase trend with increasing CNW concentration.

3.4. Spherulitic growth rate and nucleation density

Isothermal crystallization behaviors of PHBV and PHBV/CNW composites at 50, 60 and 70 °C were also studied by direct polarized optical microscopy (POM) observation. PHBV spherulites with characteristic Maltese cross could be clearly seen under POM (Fig. 9). For neat PHBV, the number of spherulites was small and their size was relatively large because there was ample space for them to grow before impinging onto each other (Fig. 9a). However, with the addition of just 1.2% CNWs, the number of PHBV spherulites increased significantly and consequently their size was dramatically reduced (Fig. 9b). Similar results were reported for PHBV with silica (Ma et al., 2008) and clay (Chen et al., 2004) nanoparticles.

The variation in dimensions of the spherulites can also be observed in the change of melting temperature of the composites. During the study of the effect of cellulose nanowhiskers on non-isothermal crystallization kinetics of PHBV (Ten et al., 2012), it was determined that equilibrium melting temperatures were reduced after the addition of CNWs, indicating hindered lamellar growth in the presence of high contents of CNWs.

The micrograph for 2.3% CNWs shows the highest spherulite density and the smallest spherulite size among all the

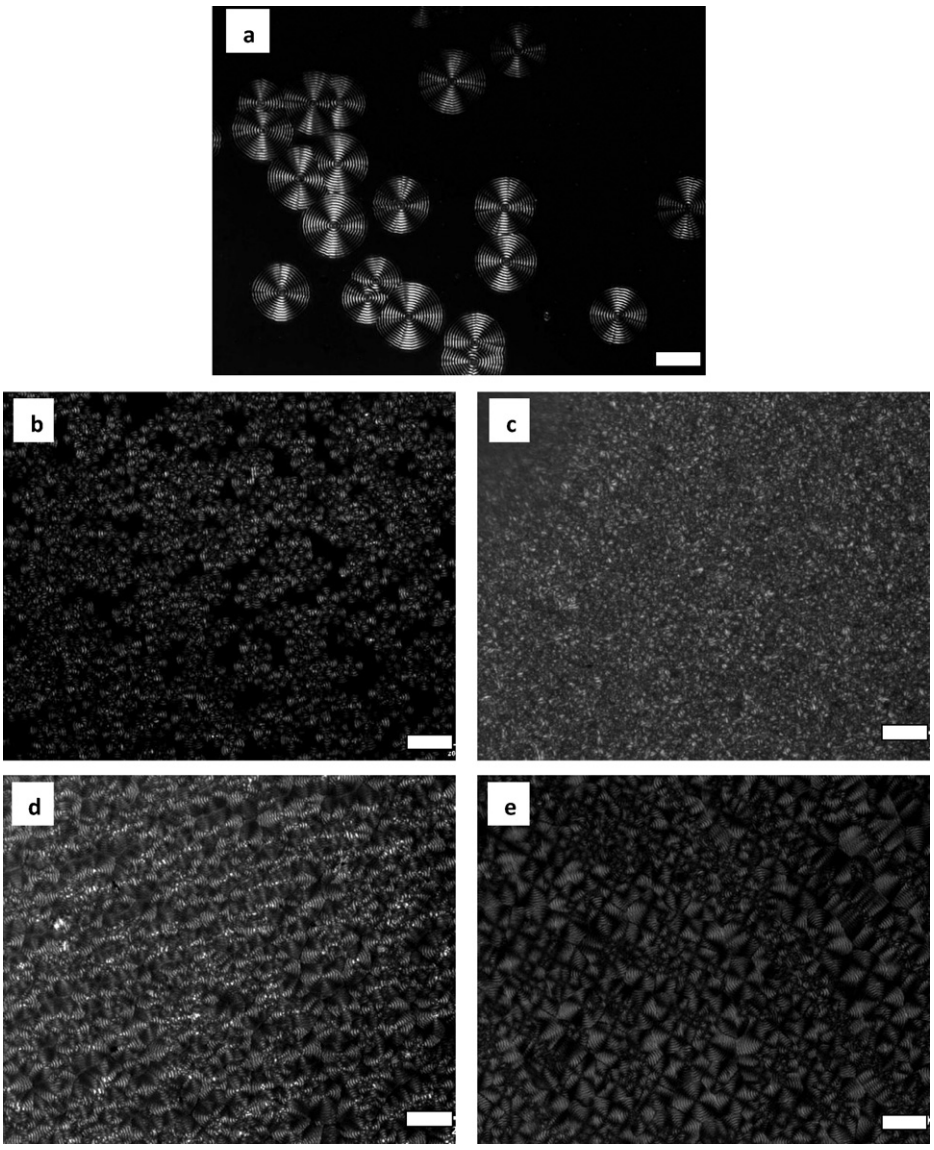

Fig. 9. POM images of isothermal crystallization of neat PHBV (a); PHBV/1.2% CNW (b); PHBV/2.3% CNW (c); PHBV/3.3% CNW (d); PHBV/4.6% CNW (e) at 50 °C. Elapsed time is 2 min. Scale bar is 20 μm.

concentrations. These POM observations clearly suggested the strong nucleation effect of CNWs. Moreover, at 3.3% and 4.6% CNW concentrations, the spherulite density decreased and the spherulite size increased (Fig. 9d and e), an indication of CNW agglomeration which caused reduced nucleation sites and increased chain diffusion. The POM micrographs taken at 60 and 70 °C (picture not shown) exhibited larger spherulites compared to at 50 °C over the same crystallization time, indicating larger spherulite growth rate at higher temperatures.

Nucleation effect of CNWs can be evaluated based on spherulitic growth rate analysis and nucleation density estimation. The spherulite growth rate G_s can be determined from time-resolved optical micrographs. The radius of spherulites grew linearly with time for all the formulations under three isothermal temperatures. This linearity of spherulite radius R suggested that cellulose nanowhiskers did not accumulate at crystal growth fronts but were trapped in the interlamellar regions of the PHBV spherulites (Chiu, 2002).

The spherulite growth rate G_s can be determined from the slopes of these spherulite radii vs. time lines. G_s for all the samples are compared in Fig. 10. The growth rate showed the same trend at all crystallization temperatures, i.e., G_s first decreased with increasing CNW concentration and then increased with the concentration. Similar results were reported for

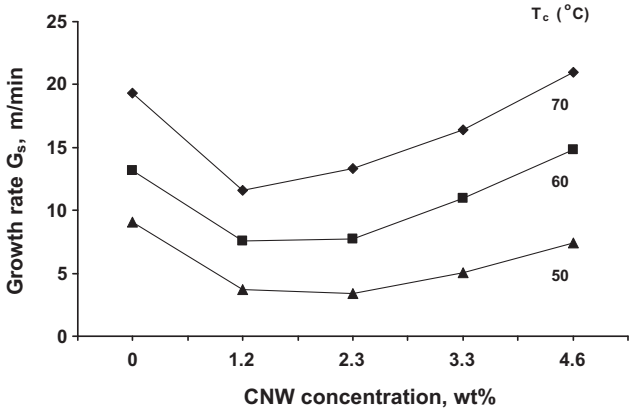

Fig. 10. Spherulitic growth rate of PHBV and PHBV/CNW composites at 50, 60 and 70 °C isothermal crystallization temperatures.

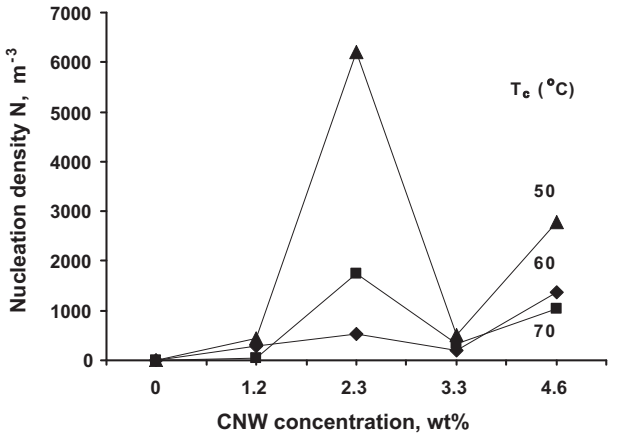

Fig. 11. Nucleation density of PHBV and PHBV/CNW composites at 50, 60, 70 °C isothermal crystallization temperatures.

multi-wall carbon nanotubes/isotactic polypropylene composites (Xu & Wang, 2008). As explained before, the decrease was due to the confinement effect of CNWs, which hindered chain diffusion and folding into crystalline lattice. CNW agglomeration at high concentrations essentially reduced the total surface area of CNWs and allowed larger degree of mobility of PHBV chains. This resulted in the increase in G_s.

Fig. 10 also shows that G_s increases with temperature. This was because PHBV chains diffused faster at high temperatures. More polymer chains were able to configure themselves into the crystalline lattice of the spherulite growth front per unit time, leading to higher spherulite growth rate.

The nucleation effect of CNWs was further confirmed by calculating nucleation density from the POM micrographs. The number of heterogeneous nuclei or the primary nucleation density N can be roughly estimated based on maximum radius of the spherulites before impingement R_m (Maiti, Nam, Okamoto, Hasegawa, & Usuki, 2002; Nam, Ray, & Okamoto, 2003):

$$N = \left(\frac{3}{4}\right)\pi R_m^{-3}, \quad (10)$$

Fig. 11 shows the variation of N under different conditions. It is evident that the nucleation effect of CNWs is most prominent at 50 °C and N peaks at 2.3% CNW. The nucleation density for PHBV/2.3 wt% CNWs is 2800 times higher compared to that of the neat PHBV. The nucleation density rebounded at 4.6% for all three temperatures. This was probably due to the wide size distribution of the spherulites as shown in Fig. 9e, which in turn was attributed to highly uneven distribution of CNWs at high concentrations.

4. Conclusion

This study investigated the effects of CNWs on the crystallization of PHBV under different crystallization temperatures and CNW concentrations. Crystallization kinetics was studied using DSC and POM. The changes in crystalline structure of PHBV with CNWs were investigated by XRD. Avrami theory was used to analyze isothermal crystallization of PHBV. The results suggested that CNW content and isothermal crystallization temperature could significantly alter crystallization kinetics of PHBV. CNWs influenced PHBV crystallization through two processes: nucleation and spherulite growth. CNWs increased PHBV crystallization rate by promoting heterogeneous nucleation when CNW concentrations were low. The crystallization rate started to decrease when the confinement effect of CNWs outweighed their nucleation effect. High crystallization rate did not always lead to high degree of crystallinity. The calculation of crystallization rate was based on the first half ($t_{0.5}$) of the whole crystallization process, where nucleation played a major role. The results derived from DSC tests were confirmed by the spherulite growth rate and nucleation density estimated from POM studies.

Acknowledgments

The authors thank Dr. Antoni Tomsia and Dr. Jijun Huang at Lawrence Berkeley National Laboratory (Berkeley, CA) for their assistance in the XRD analysis.

References

Avrami, M. (1939). Kinetics of phase change. I. General theory. *Journal of Chemical Physics*, *7*, 1103–1112.

Barham, P. J., Keller, A., Otun, E. L., & Holmes, P. A. (1984). Nucleation behaviour of poly-3-hydroxy-butyrate. *Journal of Materials Science*, *19*, 2781–2794.

Bloembergen, S., Holden, D. A., Hamer, G. K., Bluhm, T. L., & Marchessault, R. H. (1986). Studies of composition and crystallinity of bacterial poly(β-hydroxybutyrate-co-β-hydroxyvalerate). *Macromolecules*, *19*, 2865–2871.

Chan, C. H., Kummerlöwe, C., & Kammer, H.-W. (2004). Crystallization and melting behavior of poly(3-hydroxybutyrate)-based blends. *Macromolecular Chemistry and Physics*, *205*, 664–675.

Chen, G. X., Hao, G. J., Guo, T. Y., Song, M. D., & Zhang, B. H. (2004). Crystallization kinetics of poly(3-hydroxybutyrate-*co*-3-hydroxyvalerate)/clay nanocomposites. *Journal of Applied Polymer Science*, *93*, 655–661.

Chiu, H. J. (2002). Spherulitic morphology and crystallization kinetics of poly(vinylidene fluoride)/poly(vinyl acetate) blends. *Journal of Polymer Research*, *9*, 169–174.

Dagnon, K. L., Chen, H. H., Innocentini-Mei, L. H. A., & D'Souza, N. (2009). Poly[(3-hydroxybutyrate)-*co*-(3-hydroxyvalerate)]/layered double hydroxide nanocomposites. *Polymer International*, *58*, 133–141.

El-Hadi, A., Schnabel, R., Straube, E., Muller, G., & Henning, S. (2002). Correlation between degree of crystallinity, morphology, glass temperature, mechanical properties and biodegradation of poly (3-hydroxyalkanoate) PHAs and their blends. *Polymer Testing*, *21*, 665–674.

Figuly, G.D. (2004). U.S. Patent 6,774,158.

He, Y., & Inoue, Y. (2003). Alfa-cyclodextrin-enhanced crystallization of poly(3-hydroxybutyrate). *Biomacromolecules*, *4*, 1865–1867.

Hirota, Y., Yoshie, N., Ishii, N., Kasuya, K., & Inoue, Y. (2005). Correlation between solid-state structures and enzymatic degradability of cocrystallized blends. *Macromolecular Bioscience*, *5*, 1094–1100.

Jiang, L., Huang, J., Qian, J., Chen, F., Zhang, J., Wolcott, M. P., et al. (2008). Study of poly(3-hydroxybutyrate-co-3-hydroxyvalerate) (PHBV)/bamboo pulp fiber composites: Effects of nucleation agent and compatibilizer. *Journal of Polymers and the Environment*, *16*, 83–93.

Jiang, L., Morelius, E., Zhang, J., Wolcott, M. P., & Holbery, J. (2008). Study of the poly(3-hydroxybutyrate-*co*-3-hydroxyvalerate)/cellulose nanowhisker composites prepared by solution casting and melt processing. *Journal of Composite Materials*, *42*, 2629–2645.

Kamiya, N., Sakurai, M., Inoue, Y., Chujo, R., & Doi, Y. (1991). Studies of cocrystallization of poly(3-hydroxybutyrate-co-3-hydroxyvalerate) by solid-state high-resolution NMR spectroscopy and differential scanning calorimetry. *Macromolecules*, *24*, 2178–2182.

Klug, H. P., & Alexander, L. E. (1954). *X-Ray diffraction procedures for polycrystalline and amorphous materials*. New York: Wiley Interscience., p. 491.

Lai, M., Li, J., Yang, J., Liu, J., Tong, X., & Cheng, H. (2004). The morphology and thermal properties of multi-walled carbon nanotube and poly(hydroxybutyrate-*co*-hydroxyvalerate) composite. *Polymer International*, *53*, 1479–1484.

Li, L., Li, C. Y., Ni, C., Rong, L., & Hsiao, B. (2007). Structure and crystallization behavior of nylon 66/multi-walled carbon nanotube nanocomposites at low carbon nanotube contents. *Polymer*, *48*, 3452–3460.

Liu, W. J., Yang, H. L., Wang, Z., Dong, L. S., & Liu, J. J. (2002). Effect of nucleating agents on the crystallization of poly(3-hydroxybutyrate-co-3-hydroxyvalerate). *Journal of Applied Polymer Science*, *86*, 2145–2152.

Lorenzo, A. T., Arnal, M. L., Albuerne, J., & Muller, A. (2007). DSC isothermal polymer crystallization kinetics measurements and the use of the Avrami equation to fit the data: Guidelines to avoid common problems. *Polymer Testing*, *26*, 222–231.

Ma, P. M., Wang, R. Y., Wang, S. F., Zhang, Y., Zhang, Y. X., & Hristova, D. (2008). Effects of fumed silica on the crystallization behavior and thermal properties of poly(hydroxybutyrate-*co*-hydroxyvalerate). *Journal of Applied Polymer Science*, *108*, 1770–1777.

Maiti, M., Nam, P. H., Okamoto, M., Hasegawa, N., & Usuki, A. (2002). Influence of crystallization on intercalation, morphology, and mechanical properties of polypropylene/clay nanocomposites. *Macromolecules*, *35*, 2042–2049.

Martínez-Sanz, M., Olsson, R. T., Lopez-Rubio, A., & Lagaron, J. M. (2011). Development of electrospun EVOH fibres reinforced with bacterial cellulose nanowhiskers. Part I. Characterization and method optimization. *Cellulose*, *18*, 335–347.

Miao, L., Qiu, Z., Yang, W., & Ikehara, T. (2008). Fully biodegradable poly(3-hydroxybutyrate-cohydroxyvalerate)/poly(ethylene succinate) blends: Phase behavior, crystallization and mechanical properties. *Reactive & Functional Polymers*, *68*, 446–457.

Nam, J. Y., Ray, S. S., & Okamoto, M. (2003). Crystallization behavior and morphology of biodegradable polylactide/layered silicate nanocomposite. *Macromolecules*, *36*, 7126–7131.

Organ, S.J., Barham, P.J., Webb, A. (1994). US. Patent 5,281,649.

Owen, A. J., Heinzel, J., Škrbić, Ž., & Divjakovic, V. (1992). Crystallization and melting behaviour of PHB and PHB/HV copolymer. *Polymer*, *33*, 1563–1567.

Qian, J., Zhu, L., Zhang, J., & Whitehouse, R. S. (2007). Comparison of different nucleating agents on crystallization of poly(3-hydroxybutyrate-*co*-3-hydroxyvalerates). *Journal of Polymer Science Part B: Polymer Physics*, *45*, 1564–1577.

Siqueira, G., Fraschini, C., Bras, J., Dufresne, A., Prud'homme, R., & Laborie, M.-P. (2011). Impact of the nature and shape of cellulosic nanoparticles on the isothermal crystallization kinetics of poly(e-caprolactone). *European Polymer Journal*, *47*, 2216–2227.

Sugiyama, J., Vuong, R., & Chanzy, H. (1991). Electron diffraction study on the two crystalline phases occurring in native cellulose from an algal cell wall. *Macromolecules*, *24*, 4168–4175.

Ten, E., Jiang, L., Bahr, D. F., Li, B., & Wolcott, M. P. (2012). Effect of cellulose nanowhiskers on mechanical, dielectric and rheological properties of Poly(3-hydroxybutyrate-*co*-3-hydroxyvalerate) (PHBV)/cellulose nanowhiskers (CNW) composites. *Industrial and Engineering Chemistry Research*, *51*, 2941–2951.

Ten, E., Turtle, J., Bahr, D., Jiang, L., & Wolcott, M. (2010). Thermal and mechanical properties of poly(3-hydroxybutyrate-*co*-3-hydroxyvalerate)/cellulose nanowhiskers composites. *Polymer*, *51*, 2652–2660.

Tokoh, C., Takabe, K., Fujita, M., & Saiki, H. (1998). Cellulose synthesized by acetobacter xylinum in the presence of acetyl glucomannan. *Cellulose*, *5*, 249–261.

Ublekov, F., Baldian, J., & Nedkov, E. (2009). Crystalline β-structure of PHBV grown epitaxially on silicate layers of MMT. *Journal of Polymer Science Part B: Polymer Physics*, *47*, 751–755.

Weihua, K., Yong, H., & Yoshio, I. (2005). Fast crystallization of poly(3-hydroxybutyrate) and poly(3-hydroxybutyrate-co-3-hydroxyvalerate) with talc and boron nitride as nucleating agents. *Polymer International*, *54*(5), 780–789.

Withey, R. E., & Hay, J. N. (1999). The effect of seeding on the crystallisation of poly(hydroxybutyrate), and co-poly(hydroxybutyrate-co-valerate). *Polymer*, *40*, 5147–5152.

Xie, Y., Kohls, D., Noda, I., Schaefer, D. W., & Akpalu, Y. A. (2009). Poly(3-hydroxybutyrate-co-3-hydroxyhexanoate) nanocomposites with optimal mechanical properties. *Polymer*, *50*, 4656–4670.

Xu, D., & Wang, Z. (2008). Role of multi-wall carbon nanotube network in composites to crystallization of isotactic polypropylene matrix. *Polymer*, *49*, 330–338.

Zhang, Y., Yu, J. R., Zhou, C. J., Chen, L., & Hu, Z. M. (2010). Preparation, morphology, and adhesive and mechanical properties of ultrahigh-molecular-weight polyethylene/SiO_2 nanocomposite fibers. *Polymer Composites*, *31*, 684–690.

Zhou, C., Chu, R., Wu, R., & Wu, Q. (2011). Electrospun polyethylene oxide/cellulose nanocrystal composite nanofibrous mats with homogeneous and heterogeneous microstructures. *Biomacromolecules*, *12*(7), 2617–2625.